PNAS Nexus, 2024, 3, pgae288
https://doi.org/10.1093/pnasnexus/pgae288
Advance access publication 31 July 2024
Research Report

Coupled oscillations orchestrate selective information transmission in visual cortex

Mohammad Bagher Khamechian[a,b], Mohammad Reza Daliri[a,b,*,1], Stefan Treue[c,d,e,f,*,1] and Moein Esghaei[b,c,*,1]

[a]Neuroscience and Neuroengineering Research Laboratory, Biomedical Engineering Department, School of Electrical Engineering, Iran University of Science and Technology (IUST), Dardasht St., District 8, Tehran 16846-13114, Iran
[b]School of Cognitive Sciences, Institute for Research in Fundamental Sciences (IPM), Opposite the ARAJ, Artesh Highway, Aghdassieh, Tehran 1956836613, Iran
[c]Cognitive Neuroscience Laboratory, German Primate Center-Leibniz Institute for Primate Research, Kellnerweg 4, Gottingen 37077, Germany
[d]Faculty of Biology and Psychology, University of Gottingen, Wilhelm-Weber-Str. 2, Gottingen 37073, Germany
[e]Bernstein Center for Computational Neuroscience, Georg-August-Universität Göttingen, Heinrich-Düker-Weg 12, Göttingen 37073, Germany
[f]Leibniz-Science Campus Primate Cognition, German Primate Center, Kellnerweg 4, Goettingen 37077, Germany
*To whom correspondence should be addressed: Email: daliri@iust.ac.ir; treue@gwdg.de; aesghaei@dpz.eu
[1]Co-last authors.
Edited By Eric Klann

Abstract

Performing visually guided behavior involves flexible routing of sensory information towards associative areas. We hypothesize that in visual cortical areas, this routing is shaped by a gating influence of the local neuronal population on the activity of the same population's single neurons. We analyzed beta frequencies (representing local population activity), high-gamma frequencies (representative of the activity of local clusters of neurons), and the firing of single neurons in the medial temporal (MT) area of behaving rhesus monkeys. Our results show an influence of beta activity on single neurons, predictive of behavioral performance. Similarly, the temporal dependence of high-gamma on beta predicts behavioral performance. These demonstrate a unidirectional influence of network-level neural dynamics on single-neuron activity, preferentially routing relevant information. This demonstration of a local top-down influence unveils a previously unexplored perspective onto a core feature of cortical information processing: the selective transmission of sensory information to downstream areas based on behavioral relevance.

Keywords: macaque visual area MT, phase-amplitude coupling (PAC), local field potentials, neural oscillations, high-gamma oscillations

Significance Statement

Highly evolved nervous systems, such as those of the primate brain consist of complex networks of areas dynamically coordinating and routing information flow to meet momentary behavioral demands. A comprehensive understanding of the underlying processes needs a mechanistic understanding of the dynamic interaction across neuronal network and single-neuron levels. Here we propose that the directional interaction between the activity of single neurons and the neural network they are embedded in determines the behavioral output. Analyses of the coupling between different frequencies of oscillatory neural activity (corresponding to different spatial extents of information processing) confirm this account, suggesting a key behavioral role of the causal influence of network-level activity on the activity of single neurons.

Introduction

How behavior-relevant information encoded in sensory cortical areas is transmitted to high-level associative areas to enable motor responses has been a core question in neuroscience (1–4). Information processing relies on a flexible interaction between and within neuronal populations. Neuronal populations elicit characteristic oscillations in their activities, known to play a critical role in numerous cortical operations, such as stimulus processing (5–8), memory processing (9, 10), and inter-regional interactions (11–14), with the characteristic frequency of the oscillations varying depending on their functional role in cortical networks (15–18). Recent investigations have shown that the oscillatory components of the local field potentials (LFPs) provide insight into how neural activities determine behavior. Importantly, several studies in visual areas, including the medial temporal area (MT), have reported that the power of beta (10–30 Hz) (19, 20) and gamma to high-gamma (50–200 Hz) LFPs (21, 22) is predictive of the behavioral output on a trial-by-trial basis. Moreover, further investigations have shown that the strength of intra-regional (23) and inter-regional (14) gamma synchrony is linked to the magnitude of association between neural activity

Competing Interest: The authors declare no competing interests.
Received: November 24, 2023. **Accepted:** June 18, 2024

and behavior. How these oscillatory activities harness the activity of single neurons to selectively associate the most relevant sensory information to behavior remains elusive.

Oscillatory neural activities in different frequencies are not independent from each other (24), but they have been observed to be coupled, a phenomenon known as "cross-frequency coupling" (25). This phenomenon, documented across multiple cortical areas and different species, is believed to be a fundamental mechanism linking activities of different spatial scales (26). Phase-amplitude coupling (PAC), the most prominently observed form of cross-frequency coupling (27, 28), reflects the power of fast oscillations co-occurring with a specific phase of slow oscillations. PAC has been suggested to underlie the local coordination of single-neuron activity by population activity, as well as the communication between distinct areas (26, 29, 30). Several previous investigations have reported that PAC plays a functional role in cortical functions, such as attention (29, 31–33), indicative of a potential function of PAC in determining the behavior of subjects. However, such function of PAC, especially in sensory areas, has not been explored before. Recent evidence highlights the critical role of beta oscillations in information transmission and high-gamma oscillations in local processing within the dorsal visual pathway (2, 16, 18, 34, 35). We propose that the cross-frequency coupling between these oscillatory frequencies may influence the performance of attentional and perceptual decisions involving visual motion processing. Here, we studied within the extra-striate visual area MT of monkeys, if PAC correlates with the speed of behavioral responses.

Our results demonstrate that, before a visual change event, the strength of coupling between the phases of beta oscillations (10–26 Hz) and the power of high-gamma rhythms (180–220 Hz, representative of the activity of local clusters of single neurons) predicts the animal's speed in reporting the upcoming change. Importantly, we document that beta phase induces a higher causal influence on spike timing during trials the animals respond faster. We also observe that the neighboring neural subpopulations in MT are more strongly coupled in the beta range when animals respond faster. These results indicate a key functional role for the unidirectional influence of local population on single neurons' activity. We speculate that this local top-down influence of population activity (represented by beta activity) on single neurons not only gates information from the level of population towards the level of single neurons but also facilitates the selective routing and biasing of behaviorally relevant information onto downstream networks that is a central feature of how attention influences sensory information processing (36–38).

Results

We trained two rhesus monkeys to perform a visual detection task (Fig. 1). In brief, the animals had to covertly attend one (the target) of two RDPs, one placed inside and the other outside the receptive field (RF) of the recorded neuron. The monkey had to give a speeded response to a brief change in RDP direction (monkey H) or direction/color (monkey T). Overall, in 86% (monkey H) and 90.3% (monkey T) of those trials where the animals did not break their eye fixation, target changes were reported correctly (see (39) for animal H and (40) for animal T for more details on the task and behavioral results). We recorded single-unit activity and LFPs from the MT area of the two monkeys. To study the dependence of the neural activity on the monkey's behavior, we subdivided the correctly performed (hit) trials into fast and slow trials based on the animal's reaction time. To investigate the functional interaction of local neural networks underlying behavior, we calculated the strength to which high frequency oscillatory LFPs are coupled to the phase of low frequency oscillations, a measure named "PAC" (41) for different pairs of frequencies. PAC strength was calculated for a 1,000 ms time window following the stimulus onset's transient evoked activity (see SI Appendix, Extended Methods, and also Fig. S1), and compared between the trial types (fast/slow) (Fig. 2A and B). We found that in fast trials, the power of high-gamma (180–220 Hz) oscillations is significantly more coupled to the phase of beta oscillations (10–26 Hz) compared to slow trials.

Beta-high gamma PAC predicts the speed of animal's response

We measured the PAC strength for fast and slow trials where the target stimulus change occurred inside the RF, using a modified version of the method previously introduced (41) (see SI Appendix, Extended Methods). This measure ranges from 0 to 1.

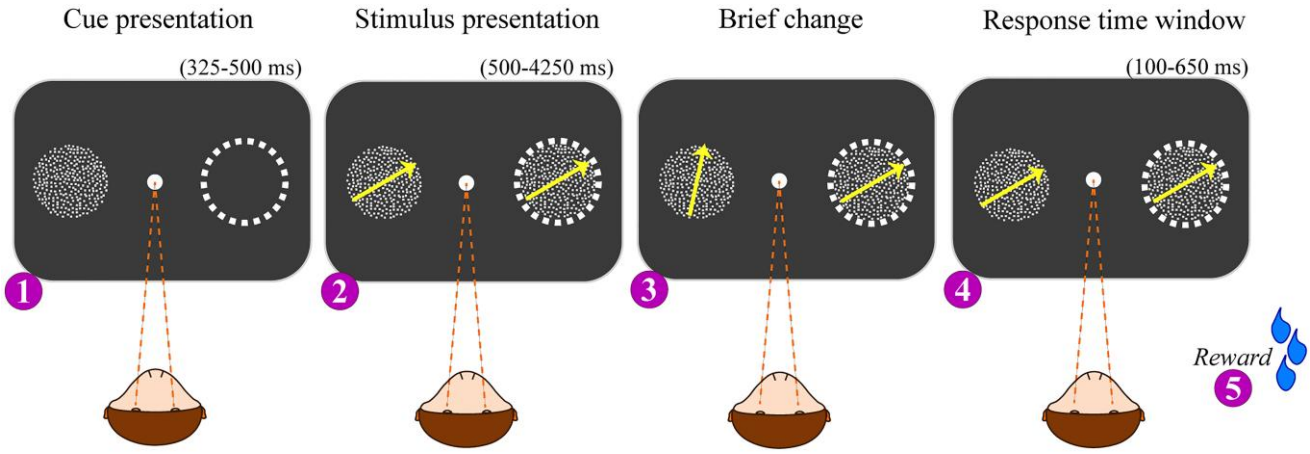

Fig. 1. Behavioral paradigm. To start a trial, the monkey pressed a lever bar and maintained their gaze on a fixation point (filled circle or filled square for monkey H and T, respectively). Next, a static RDP (moving RDP for monkey T) appeared for 325–500 ms to signal (cue) the position of the target stimulus on the screen. After ending the cue exhibition period, two moving RDP stimuli were displayed for a random duration of 500–4250 ms. Next, a quick direction change (direction or color change for Monkey T) occurred in one of two RDPs and the monkey was instructed to release the lever bar within a response window of 100 to 650 ms. White dashed-circle was not displayed on the real behavioral task, yet it was employed for a representative purpose, to delineate the RF location of MT neurons on the monitor screen. The inset numbers implicate the behavioral task sequences.

It is 0 when there is no systematic relation between the phase of the low frequency and the power of the high frequency component, and it equals 1 when the power of the high frequency component is fully aligned with the phase of the low frequency component. To calculate PAC for the fast and slow trials, we filtered the LFPs into different low and high frequency bands. For the low frequencies, LFPs were filtered using nonoverlapping band-pass filters with the width of 2 Hz, ranging between 1–30 Hz and for high frequencies, LFPs were filtered using 10 Hz wide band-pass filters overlapping by 5 Hz within the range of 35–255 Hz. Next, the instantaneous phases of the low frequency components were calculated by applying a Hilbert transform on the filtered signals and the instantaneous power of the high frequency components were estimated by calculating the envelope of the filtered signals (see SI Appendix, Extended Methods). This procedure provided 15 and 43 time-series for the instantaneous phases and powers, respectively for each trial's LFP. We next calculated the PAC strength for all pairs of low and high frequency components. This yielded a 2D matrix with 43×15 PAC elements for each trial's LFP. Figures 2A and B shows the difference between the average PAC maps for fast and slow trials (see also Fig. S2 for the PAC of trials with moderate RTs). The X- and Y-axes represent the value at the center of each frequency band and colors indicate the levels of difference in PACs (fast–slow). Our data clearly show that the coupling of high-gamma power (~180–220 Hz) to beta phase (~10–26 Hz) is higher in fast compared to slow trials (using two-sided Wilcoxon rank sum test with FDR correction for multiple testing; $\rho < 0.0039$ and $\rho < 0.0042$ for monkeys H and T). To avoid the side-effect of LFP power on the accuracy of PAC's calculation, for Fig. 2A and B, we selected the fast and slow trials with no significant difference between their beta power (15–25 Hz) (monkey H: $\rho = 1$, Monkey T; $\rho = 0.996$ using two-sided Wilcoxon rank sum test), using a histogram-based method (see SI Appendix, Extended Methods). We also conducted a similar measurement of PAC for trials where the target change occurred outside the RF. This showed no significant difference within the frequency ranges depicted in Fig. 2A and B (see Fig. S3, $\rho > 0.05$ using a two-sided Wilcoxon rank sum test, corrected for multiple comparisons using FDR), suggesting that the increase of PAC strength in fast trials is not due to differences in neuronal excitability levels or potential changes in the monkey's arousal level. We also observed that the PAC difference predicted the trial type more strongly (monkey T) or as strongly as (monkey H) the spike rates do (Fig. S4). We also ensured that the PAC difference within the beta-high gamma (HG) pairs was not due to a systematic difference between HG powers; the average strength of high-gamma power (180–220 Hz) was either significantly stronger in the selected slow compared to fast trials or did not have any significant difference (monkey H: $\rho < 10^{-10}$ two-sided Wilcoxon rank sum test, monkey T: $\rho > 0.4$ two-sided Wilcoxon rank sum test). The PAC differences also were not subject to a potentially significant dependency on the target stimulus's preferred or antipreferred direction of motion (see Fig. S5 for more details). It should be noted that the strength of the high-gamma power is dissociated from the spectral leakage of spike into LFP (see Refs (2, 34, 42)). We further showed that the high-gamma power has a significant negative correlation with the animal's RT (monkey H: $r = -0.05$, $\rho < 0.01$, monkey T: $r = -0.1$, $\rho = 0.05$, Spearman correlation, two-sided Wilcoxon signed rank test, see Fig. S6 for more details). To visualize beta-HG coupling, we calculated the normalized power of high-gamma at different beta phases for fast and slow trials, pooled across the two animals (Fig. 2C) (see SI Appendix, Extended Methods). The result clearly shows that for fast trials, high-gamma power is distributed nonuniformly across beta phases for both monkeys, while this nonuniform dependence is clearly smaller for the slow group. This suggests that the local neural activity reflected by HG more strongly follows the beta phase in fast compared to slow trials, presumably for the sensory activities to be more organized in time. We further measured the beta-coupling of neighboring sites recorded simultaneously, for the two behavioral conditions. Figure 2D shows the aggregated phase locking values (PLVs) for both monkeys for the fast and slow trials, suggesting that the phase synchronization among neighboring neurons is significantly larger for faster responses ($\rho < 0.00098$using two-sided Wilcoxon rank sum test). To confirm this, we examined the synchrony among pairs of neurons by measuring the cross-correlogram between the spiking activities of neurons recorded simultaneously from two different electrodes (Fig. S7). These results indicate that neighboring neurons fire significantly more synchronously within beta frequencies during fast rather than slow responses ($\rho < 0.005$, permutation test). We further calculated the circular histograms of the spike-triggered "beta phase" for the fast and slow trials (Fig. S8). The results indicate that neurons fire selectively within a certain phase range in fast trials, while this selectivity is absent in slow trials ($\rho < 0.00021$, fast trials; $\rho > 0.13$, slow trials; Rayleigh test). Furthermore, an analysis of power spectral density shows a spectral peak relative to the aperiodic components in the beta frequency range for both monkeys (Fig. S9 C and D). These sets of evidence suggest that not only the neural activity confined to local circuitries is more coupled to beta, but neighboring neural circuits are also more strongly coupled via beta, in fast trials. This argues that the beta rhythm may be crucial for the efficient transmission of information towards downstream areas involved in generating the behavioral output. To examine the argument, we compared the high-gamma power between the peaks and troughs of the beta rhythms. To this end, the time-frequency spectrogram was computed for the high-gamma frequency range (160–250 Hz) using raw LFPs time-locked to the maximum beta (17–21 Hz) peak (see SI Appendix, Extended Methods). It is visually evident that the high-gamma power is stronger at the troughs compared to the peaks (Figs. 2E and S10). To quantify this difference, we calculated the high-gamma modulation index (M_{HGp}): $M_{HGp} = (P_{peak} - P_{trough})/(P_{peak} + P_{trough})$, where P_{peak} and P_{trough} represent the HG power at the peak and trough of the beta rhythm, respectively (see SI Appendix, Extended Methods). The result demonstrated that the strength of high-gamma power in beta troughs is significantly larger than in beta peaks on a trial-by-trial basis ($M_{HGp} = 0.25$, $\rho < 0.0001$, permutation test).

Different dynamics of PAC in fast and slow trials reflect network delay in routing information

We documented that high-gamma fluctuations are more strongly coupled to the phase of the beta oscillations when an animal responds faster. To study the temporal dynamics of this coupling, PAC was further calculated for different time windows relative to the target change. To this end, we focused on the LFPs within the 1,000 ms window before the target change and calculated the strength of beta-HG PAC (for frequency pairs with PAC shown to be significantly linked to reaction time—marked by white lines in Fig. 2A and B). We used a 400 ms-wide window sliding with steps of 10 ms, to calculate the time-resolved PAC for the fast and slow trials (see SI Appendix, Extended Methods) (Fig. 3). X-axes represent the value at the center of the sliding window in each step, and Y-axes indicate the PAC strength averaged across the

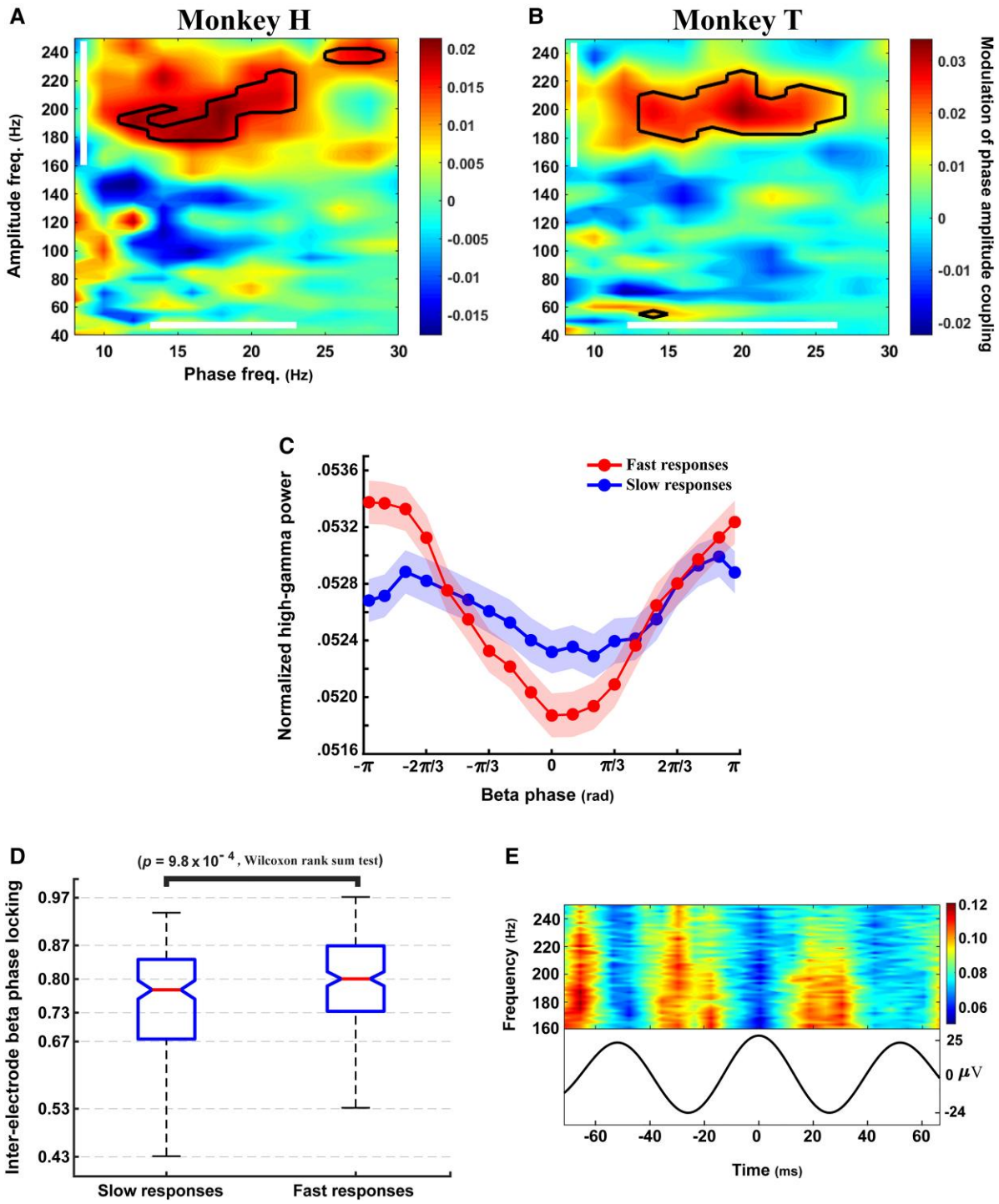

Fig. 2. Strength of PAC differs between fast and slow behavioral responses. A, B) Maps of differences between PAC strengths are calculated for 15(phase providing)*43(power providing) pairs of frequency bands calculated from nonoverlapping 2 Hz pass-band windows (changing between 1 and 30 Hz) and 10 Hz pass-band windows overlapping with 5 Hz bounds (changing between 35 and 255 Hz), respectively. The heat maps show the average PAC strength of slow trials subtracted from that of fast trials. X-/Y-axes indicate the lower bound of phase-providing/power-providing frequency bands. Black outlines demonstrate frequency pairs with a significant PAC difference between the fast and slow trials ($\rho = 0.0039$ and $\rho = 0.0042$ for monkeys H and T, respectively; two-sided Wilcoxon rank sum test with FDR correction for multiple comparisons). The phase-providing and power-providing frequency ranges with a significant behavioral modulation are indicated by white lines for each animal C, Normalized average of high-gamma power (160–250 Hz) within different phases of the beta band (19 nonoverlapping phase segments) averaged across animals. The beta frequency band was selected between 13–23 Hz/12–26 Hz for monkey H/T (frequencies with a significant PAC modulation-according to maps A/B). X values represent the middle of the phase segments and error bars show the SEM. D, The boxplot illustrates the phase locking value (PLV) of the oscillations within the beta band between pairs of sites (averaged across beta sub-bands, see SI Appendix, Extended Methods), recorded simultaneously for the two animals. The PLV indicates an average difference of instantaneous phases between two neighboring electrodes. PLV was significantly different between the fast and slow trials ($\rho = 0.00098$ two-sided Wilcoxon rank sum test). E) Beta peak-triggered spectrogram for high-gamma. The spectrogram was calculated using short-time Fourier transform with 7 ms time windows of 1 ms overlaps. Both fast and the slow trials are pooled together here across both animals. Color bar scales between the minimum and maximum of the normalized powers across high-gamma frequencies. The bottom curve shows the beta-filtered LFPs (17–21 Hz) averaged across trials after aligning to their highest-amplitude peak.

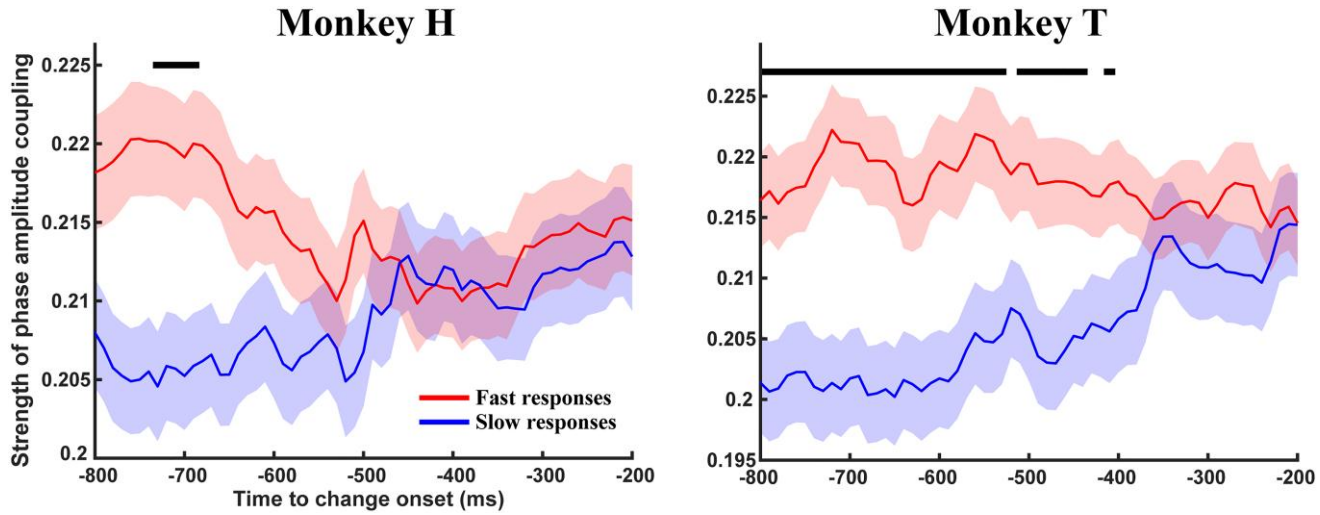

Fig. 3. Time-resolved changes of PAC strength within the 1,000 ms before the direction change. 400 ms sliding time windows, lagged by 10 ms were used for calculating the PAC strength within those frequencies, with their PACs significantly differentiated across reaction times (as shown in Fig. 2A and B). X values represent the middle of the analysis time windows. The black line marks time windows with a significant difference in PAC between fast and slow trials (monkey H: $\rho = 0.0039$ and monkey T: $\rho = 0.0294$; two-sided Wilcoxon rank sum test, corrected for multiple comparisons using FDR).

significantly modulated frequency pairs (marked by white lines in Fig. 2A and B). These results indicate that the PAC strength starts to be significantly different between fast and slow trials long before the target change and remains apart until at the latest 400 ms before the change onset (monkey H: $\rho < 0.0039$ and monkey T: $\rho < 0.0294$; two-sided Wilcoxon rank sum test, corrected for multiple comparisons using FDR). Although we observed a difference of target change latency between fast and slow trials in one of the animals (fast > slow for monkey H, $\rho < 2 \times 10^{-4}$; [$\rho > 0.33$ for monkey T]; two-sided Wilcoxon rank sum), the PAC difference before change onset is not due to such a difference in the target change latency (see Fig. S11 for details). This indicates that the PAC differences may not be due to different adaptation levels. These results suggest that the potential influence of beta-HG coupling on the efficiency of sensory processing may involve multisynaptic, rather than mono-synaptic circuits. This indicates that it may be the transmission of visuomotor information (as a cross-areal, rather than a within-area process), that is influenced by the strength of PAC. One possibility could be that PAC causes an improvement of inter-areal communication channel with downstream areas (30, 42).

High-gamma activity correlates with spikes on a trial-by-trial basis

Our observation of the link between beta-HG coupling and behavior, is in line with previous reports highlighting the role of PAC in information transmission between cortical areas; suggesting that area MT transmits sensory information using the high frequency oscillatory activity, HG oscillations, after synchronizing with downstream areas in the beta band (29, 30). This implies that the HG oscillatory activity should be correlated with the spiking activity. To test this, we pooled the fast and slow trials and measured the correlation between spike rate and high-gamma power (180–220 Hz) across trials (monkey H; $r = 0.12$, $\rho = 1.1 \times 10^{-5}$ and monkey T; $r = 0.37$, $\rho = 2.7 \times 10^{-27}$, Spearman rank method, see Fig. 4A) (see SI Appendix, Extended Methods). To rule out a potential effect of sample size (i.e. large number of trials) on the correlation results, we also examined the relationship between the high-gamma power and the spike rate at the level of single neurons (see Fig. S12A and B for details). The correlations remained significant over single neurons' activities recorded from each animal (monkey H; $r = 0.25$, $\rho = 2.6 \times 10^{-13}$ and monkey T; $r = 0.6$, $\rho = 5.3 \times 10^{-6}$, Spearman correlation, two-sided Wilcoxon signed rank test). This positive correlation (not attributed to the spike leakage on LFP (2, 34, 42) also see Fig. S12C), is in line with previous studies (26) suggesting that high-gamma may temporally influence the spike rate of individual neurons and consequently the inter-neuronal synchrony. This spike rate-HG link further suggests that the enhancement of beta-HG coupling at faster reaction speeds (Fig. 2C) causes individual neurons to fire more intermittently and coupled to the beta phase and consequently more synchronously relative to the beta phase (Fig. 4B vs. Fig. 4C).

An enhanced orchestration of single neurons by the surrounding network in fast trials

We next asked if the relative causal influence of beta oscillations on the spikes (rather than the influence of spikes on the phase) is stronger in fast, compared to slow trials. One previously introduced approach to theoretically measure the directional interaction between an oscillatory signal and a point process (as on LFPs and spikes, respectively) is to compute the across-trial similarity of the oscillatory signal's instantaneous phase surrounding the point process (43); a larger causal influence of the oscillatory activity on spikes would be reflected by a larger phase similarity preceding the spikes, compared to after spikes. Similar to a previous study (44), we employed this technique to measure the directional interaction between the beta phase and spikes (see SI Appendix, Extended Methods, and Fig. S13). We computed the difference between the post-spike and prespike phase similarity in beta to quantify the degree to which spikes influence the beta oscillations, or vice versa, a measure named "directional interaction." To examine if this directional interaction varied as a function of response time, we subtracted the directional interaction in fast trials from that of slow trials (Fig. 5 and see SI Appendix, Extended Methods). Correspondingly, positive values (y-axis) indicate a stronger relative influence of the phase on spikes in fast trials compared to slow trials, while negative values reflect a higher relative influence in slow trials. The positive value across all times surrounding the spike event time ($p < 0.5$ for times

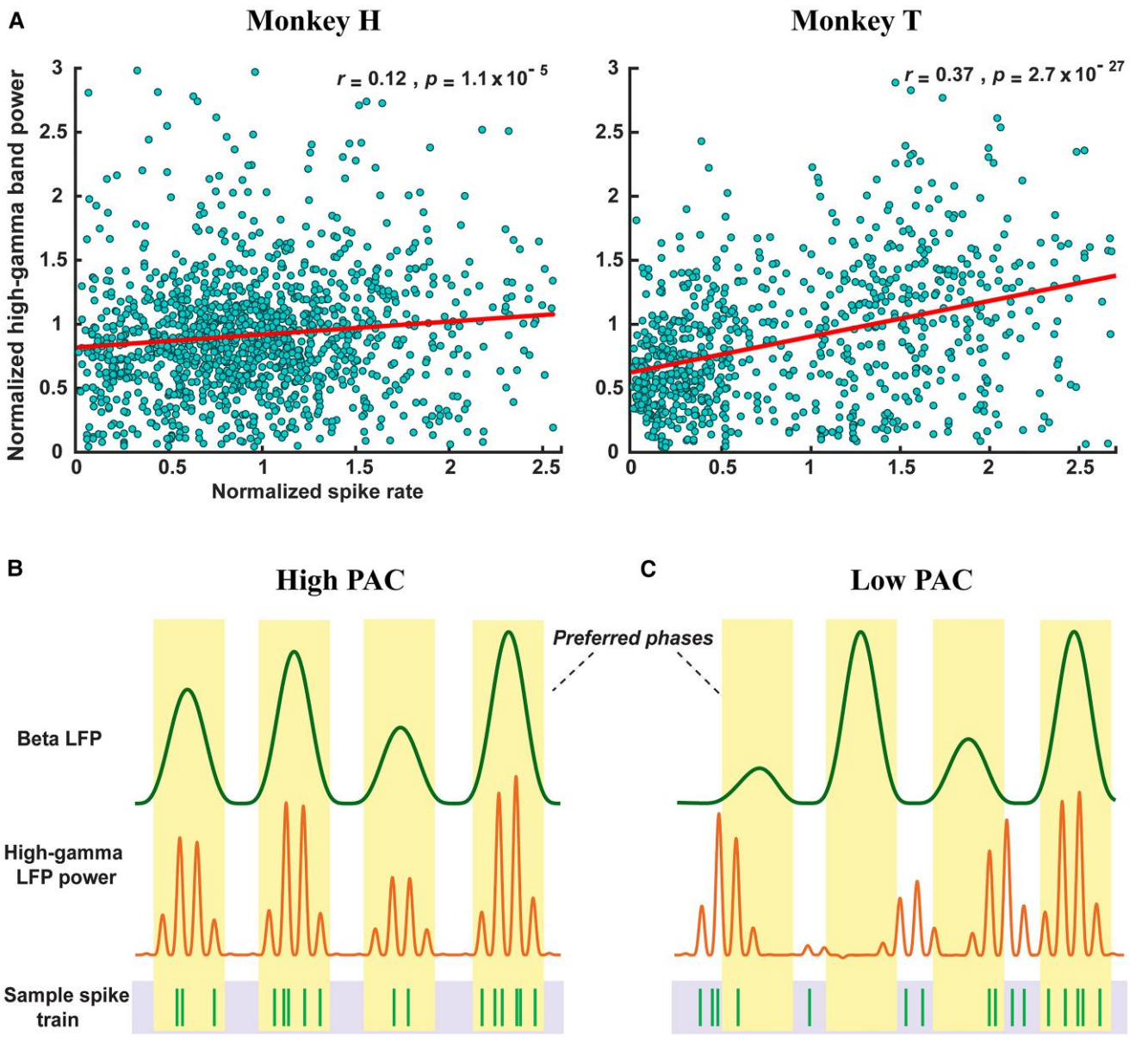

Fig. 4. Correlation between high-gamma power (180–220 Hz) and spike rate. A) Each data point represents the normalized high-gamma power (Y-axis) as a function of the associated spike rate (X axis), calculated for each trial. The high-gamma power is significantly correlated with the spike rate across trials (monkey H; $r = 0.12, \rho = 1.1 \times 10^{-5}$ and monkey T; $r = 0.37, \rho = 2.7 \times 10^{-27}$, Spearman correlation). Trials with a spike rate or high-gamma power exceeding mean ± 2×standard deviation were removed from this analysis. B and C) Cartoon rendition showing how a difference in the strength of beta-HG coupling causes spikes to be coupled (B) or de-coupled (C) from the beta phase.

beyond 10 ms from the spike event, permutation test, see SI Appendix, Extended Methods) is consistent with a more strongly pronounced role of the visuo-motor neural network (mediated by beta oscillations) when generating spikes for faster, compared to slower behavioral responses. This suggests that beta reverbration outflowed from the visuo-motor network influences the timing of MT neurons' responses significantly more strongly in fast trials, compared to slow trials.

Behavioral enhancement of PAC and neural discrimination are independent

Previous studies have shown that visual attention influences information processing via at least two basic strategies: (i) enhancing neural discriminability via increasing signal-to-noise ratio of neural responses (45–48); (ii) enhancing the inter-areal neural communication to route the most relevant behavioral information (11, 49, 50). It is unclear whether attention deploys the beta-HG coupling observed here to enhance the neural discrimination, or to improve the inter-areal communication. To answer this, we next asked the two following questions: (i) How does neural discriminability differ between fast and slow trials in our data? (ii) Is the modulation of beta-HG coupling involved in such potential neural discrimination changes?

1. To this end, we determined the single-unit activity for fast and slow trials within the same time window the PAC effect was observed. We next calculated the separability of spike rates between the preferred and antipreferred direction for

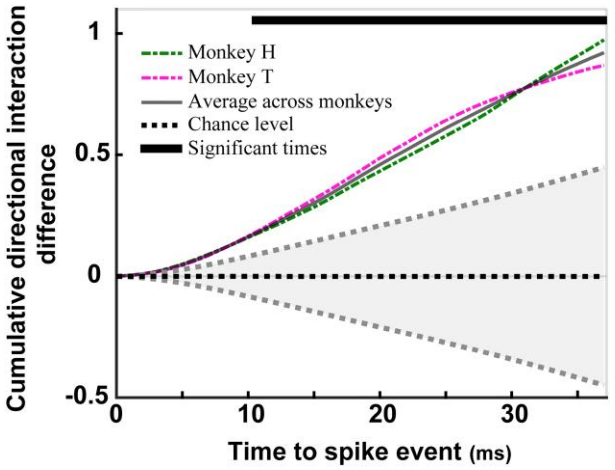

Fig. 5. Beta phase's directional interaction with spikes differs between fast and slow trials. We computed the relative directional interaction of the beta phase and the spikes computed within different time frames from the spike event. The y-axis represents the relative directional interaction in fast trials subtracted by the relative directional interaction in slow trials. Error bars reflect the standard deviation (SD) estimated by repeatedly shuffling the trial labels (fast/slow) ($N = 1{,}000$).

individual neurons for each trial type, using an ROC analysis (see SI Appendix, Extended Methods) (Fig. 6A). The area under the ROC curve (AUC) analysis and permutation hypothesis testing between the preferred and antipreferred stimuli showed that the neural discriminability is significantly larger in fast, compared to slow trials ($\rho = 0.027$ and $\rho = 0.008$ in monkeys H and T). The difference in the neural discriminability is not due to disparities between the fast and the slow trials in the stimulus-evoked transient activity (see Fig. S1). This suggests that the sensory information is encoded more effectively when the animal responds faster, presumably due to a higher level of attention (49, 51, 52) (see Fig. 6B for a schematic of the data).

2. We investigated the potential interaction of beta with HG PAC and neuronal discrimination on a trial-by-trial basis for two random trial groups with the same average reaction time. To this end, we randomly partitioned all trials into two subsets, which were not significantly different in their average reaction time ($\rho = 0.79$and $\rho = 0.99$ for monkey H and T respectively, two-sided Wilcoxon rank sum test), while they were significantly different in their beta-HG PAC strength ($\rho = 1.1 \times 10^{-3}$and $\rho = 1.7 \times 10^{-4}$ for monkey H and T, respectively, two-sided Wilcoxon rank sum test) (see SI Appendix, Extended Methods). Next, we calculated the neural discrimination between the preferred and antipreferred direction for each trial group using the ROC approach. The corresponding ROC curves and the probability density of high-gamma amplitude relative to beta phases for the two chosen subsets (high-PAC trials vs. low-PAC trials) are shown in Fig. 6C and D. Our AUC analysis and the permutation hypothesis testing between the preferred and antipreferred directions of motion demonstrate that the neural discrimination is not significantly different between the high-PAC and low-PAC trial groups ($\rho = 0.72$ and $\rho = 0.30$ for monkeys H and T, AUC values: [0.97, 0.973] and [0.98, 0.964] for [high-PAC, low-PAC trials] for monkeys H and T, respectively). This suggests that PAC and neural discrimination are independent predictors of behavior, indicating that they incorporate different neural mechanisms to influence the visuo-motor performance.

Computational model confirms the role of PAC in inter-areal connectivity

To further validate our experimental findings, we designed a modeling framework to elucidate how upstream cortical areas (e.g. MT) could communicate effectively with downstream associative areas (e.g. LIP), through beta-high-gamma PAC. Assuming a constant beta phase locking between the downstream and upstream areas, we asked if different PAC strengths in the upstream area lead to different levels of functional connectivity with the downstream area. To this end, we generated synthetic signals with different PAC strengths representing the LFP in the upstream area, and calculated the temporal correlation (Pearson's method) of the high-gamma power with that of the downstream area (which had a constant PAC across conditions; 100%, see SI Appendix, Extended Methods) (Fig. 7A). Results show an increased high-gamma power correlation between the upstream and downstream area at stronger PACs. This also holds true for different noise levels in the upstream area. These suggest that a stronger PAC may provide two areas with an enhanced overlap between their windows of local activity (reflected by high-gamma), consistent with a previously suggested role of PAC in inter-areal communication (30).

We next examined if different PAC strengths cause differential levels of spike rate-based neural discrimination. Based on our observation of a significant correlation between high-gamma power and spike rate, we generated spike trains corresponding to the synthetically generated signals with different PACs (see SI Appendix, Extended Methods). Shannon entropy was computed next for these spike trains as a proxy for spikes' information capacity under different PAC strengths. Results show no significant dependence of entropy on PAC strength (Fig. 7B), consistent with our experimental data indicating independent mechanisms underlying the spike rate-based neural discrimination and inter-areal functional connectivity. Our evidence is therefore in line with the account that PAC is involved in inter-areal communication within the brain (7, 31, 53), with higher PACs leading to faster behavioral responses.

Discussion

Neural processing of sensory information relies on flexible routing via intra- and inter-areal interactions of neuronal populations. Here, we show evidence suggesting that key to this mechanism, is the gating influence of the local population activity on the activity at the level of single neurons. We studied the impact of neural oscillatory activities (representative of local neuronal activity) on the neuronal activity at the level of local neuronal clusters and examined the behavioral role of these oscillations within the visual cortex of monkeys. Our data and computational modeling results show that (i) the amplitude of high-gamma activity (180–220 Hz) is coupled to the phase of oscillatory neuronal activity within the beta range (10–26 Hz), in visual cortical area MT; (ii) this coupling predicts the animal's behavioral reaction times, i.e. the magnitude of attentional engagement; (iii) the strength of phase synchrony between neighboring sub-populations within the beta range predicts upcoming reaction time; (iv) fast behavioral responses entail a stronger relative causal influence of beta oscillations on spike timing; (v) this network single-neuron interaction could play a preparatory role,

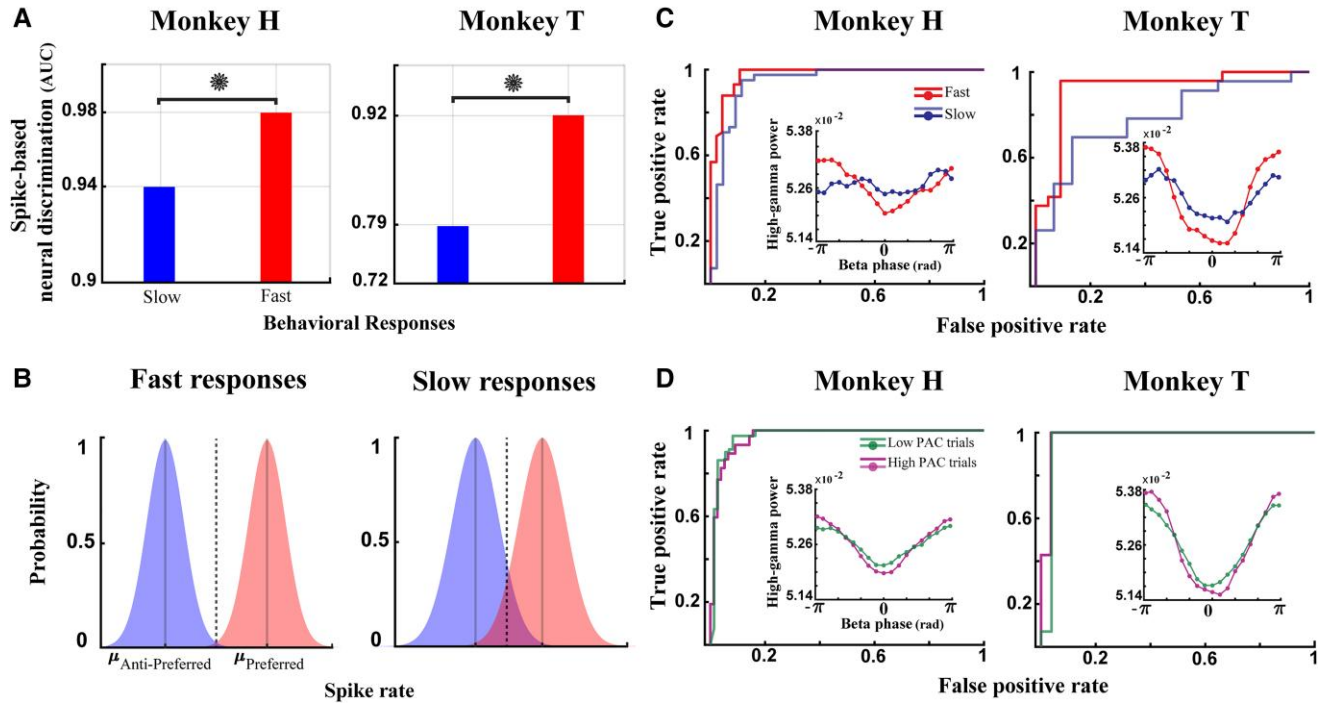

Fig. 6. Neural discrimination and PAC modulate behavior, independently. A) Bars indicate the AUC for the discrimination of preferred and antipreferred direction of motion based on spike rates (separately performed for fast and slow trials). To evaluate the significance of differences between the AUCs of fast and slow trials, permutation hypothesis testing was performed ($\rho = 0.027$ and $\rho = 0.008$ for monkeys H and T—see Materials and methods section for details). B) Cartoon representation of the spike probability distribution in fast (right panel) and slow (left panel) trials when the stimulus moves in the preferred (red) or antipreferred (blue) direction. X-values represent the spike rate and Y-values indicate the probability of a given spike rate across neural population. C) ROC curves (for the discrimination of preferred vs. antipreferred direction of motion) and probability density of high-gamma relative to the beta phase for fast and slow trials (corresponding AUCs were shown in Fig. 6A). D) Neural discrimination of the two subsets of trials with a maximum difference between their average PAC strength and a minimum difference in their average reaction times. The two subsets were found to not have a significant difference in their average reaction time (two-sided Wilcoxon rank sum test, $\rho = 0.79$ and $\rho = 0.99$ for monkeys H and T, respectively), while they were significantly different in their average PAC strength (two-sided Wilcoxon rank sum test, $\rho = 1.1 \times 10^{-3}$ and $\rho = 1.7 \times 10^{-4}$ for monkeys H and T, respectively). AUCs and a permutation test show that the neural discrimination is not significantly different between the high-PAC and low-PAC trials ($\rho = 0.72$ and $\rho = 0.30$ for monkeys H and T, respectively). The AUC analysis for high-PAC trials and low-PAC trials resulted in AUCs of (0.970 [high PAC], 0.973 [low PAC]) and (0.980 [high PAC], 0.964 [low PAC]) in monkeys H and T, respectively.

enabling the visual cortex to more efficiently transmit behaviorally relevant information to downstream cortical areas; (6) neural discrimination of sensory stimuli is predictive of the upcoming behavioral reaction time; and (vii) neural discrimination and beta-HG coupling involve independent mechanisms to enhance behavior under attention.

Our observation that the neural discrimination was predictive of the upcoming behavioral reaction time is in line with the hypothesis that attention may improve behavior via improving the neural encoding mechanisms in the fast, rather than slow trials. This effect may itself stem from the increase of neuronal discharges in fast vs. slow trials which is difficult to examine here, given our data size. The non-normal distribution of reaction times (Fig. S14) allows for the possibility that fast and slow reaction times (i.e. the two tails of the distributions) represent two independent processes; fast responses may reflect fast sensorimotor transformation, while slow responses may indicate more complex and higher level cognitive processes (54). Our results further show that the influence of PAC vs. neural discrimination on behavior use independent mechanisms. This suggests that there are at least two distinct neural processes underlying the attentional enhancement of behavior, one via enhancing the neural discrimination and the other through improving the local top-down modulatory signal (by increasing the beta-HG PAC). These two mechanisms may also underlie the behavioral component of other cognitive functions, such as memory and perceptual decision making, a question left to future studies.

Beta as a top-down regulator of visuo-motor behavior

Our observations of (i) a higher beta phase locking, (ii) a higher beta-HG coupling, and (iii) stronger relative causality of beta phase on the spike timing for fast compared to slow responses, suggest that beta oscillations sourcing from the fronto-parietal attention-control network (18, 55, 56) adaptively drive the bottom-up signals of MT neurons to more effectively guide behavior depending on the focus of spatial attention (Fig. 7C). This is in line with previous studies in sensory areas including MT showing the influence of beta rhythms on the efficacy of feed-forward projections (16–18, 55, 57).

Beta-HG coupling as a control parameter of predictive coding

It has been shown before that the feed-forward and feed-back signal projections relay sensory predictions and prediction errors, respectively, so called "predictive coding" (16, 58). This elucidates that high-level cortical areas continually generate predictions based on the incoming activity and the prior evidence, projecting these predictions to the sensory cortical areas. Sensory areas

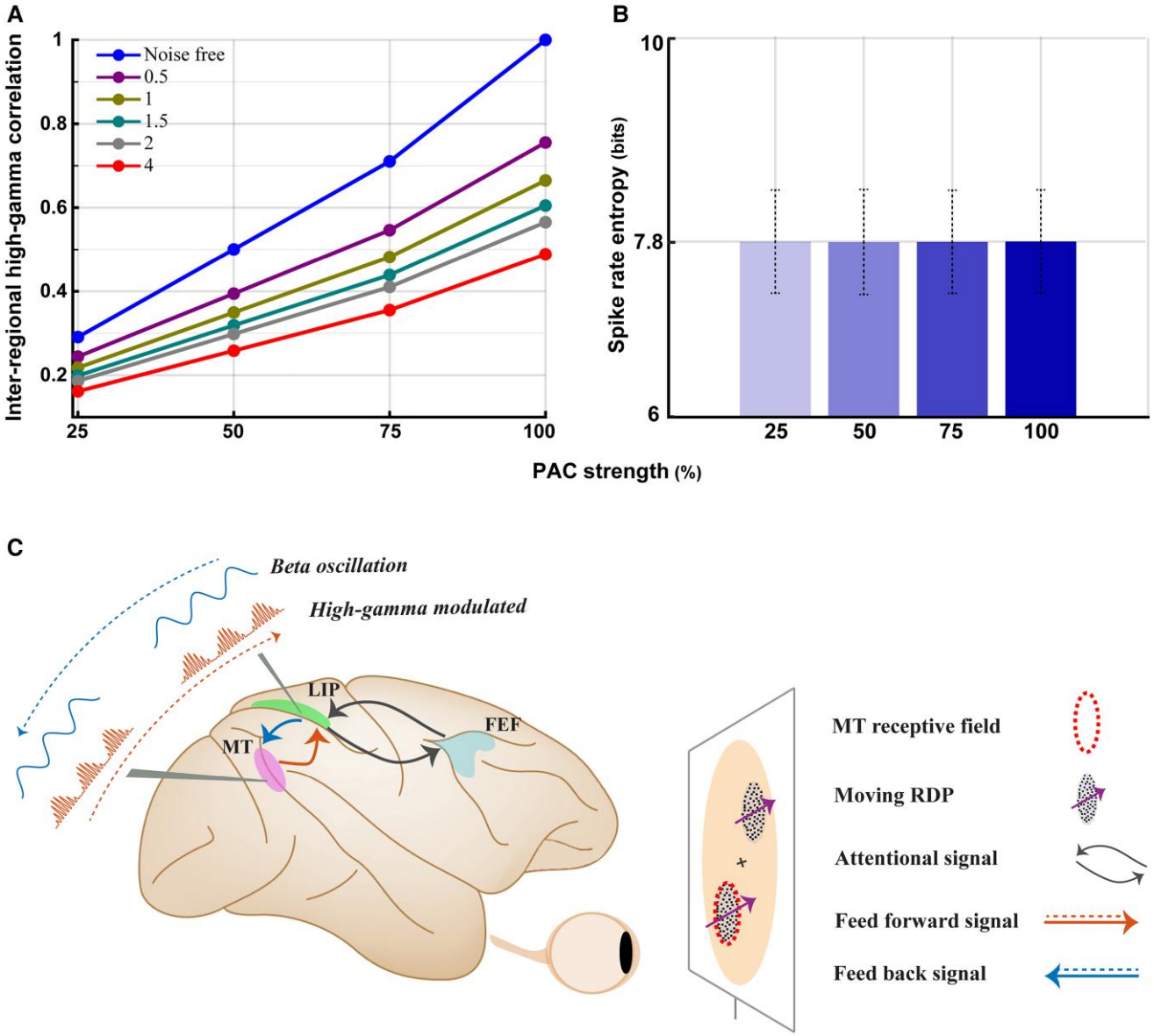

Fig. 7. Beta-HG PAC underlies inter-areal communication, independent of spike rate-based neural discrimination. A) Modeling results for the inter-areal high-gamma power correlation as a function of PAC strength; the y-axis shows the correlation of high-gamma power (modulated by the beta phase) between upstream (e.g. MT) and downstream (e.g. LIP) cortical areas. Colors illustrate different levels of additive noise magnitude; a larger value reflects a higher magnitude of additive noise (see SI Appendix, Extended Methods). B) Information capacity of spiking activity across different strengths of PAC; the y-axis shows the average Shannon entropy across 10,000 spike trains (see SI Appendix, Extended Methods). Error bars represent the standard deviation. The x-axis in (A) and (B) shows different PAC strengths, with 100% representing the highest possible PAC. C) Schematic description of inter-areal communication for transmission of the behaviorally relevant information. The top-down attention signal is believed to be mediated by a beta band oscillation generated within the LIP-FEF network. This beta activity (as a feed-back signal) may facilitate the feed-forward signal transmission from MT towards LIP, depending on the focus of attention. PAC (between beta and HG) has a facilitative role in routing sensory information across the visuo-motor network.

then estimate the prediction error by subtracting predictions from the current sensory information, and forward it to the downstream high-level area. Functionally, since predictions are updated within a longer interval, compared to the error's computation, they are suggested to involve neural activities within a lower frequency, while the transmission of prediction errors involves oscillations of higher frequencies (17, 59). Our finding of a higher beta-HG coupling in faster responses, is consistent with the predictive coding model, further suggesting that a higher temporal coordination of beta (corresponding to the top-down signal) and HG (corresponding to the bottom-up signal) may contribute to the integration of the prediction and the prediction error.

Local interneuron co-activation mediates bottom-up routing of visuo-motor information

Recent studies in rodents and humans have documented that intrinsic properties of interneurons underlie high-gamma brain rhythms (25, 60–63). The network of such co-active interneurons then imposes a rhythmic inhibition on excitatory pyramidal cells to discharge in phase with the interneuron population's

rhythm (62). Further studies have demonstrated that high-gamma activities (e.g. ripple activities), shaped by local cortical circuits (27), are involved in high-level cognitive functions, such as planning (64), decision making (65) and memory consolidation (9). Specifically, a study using intracranial recordings in the human cortex, has identified a widespread synchrony within the high-gamma range of 50–125 Hz and frequencies above (>125 Hz) across the primary visual cortex, limbic and higher order cortical regions, during memory encoding and recalling tasks (10). Further, recent investigations in the hippocampus and neocortex have indicated that sub-populations of interneurons oscillating at faster and slower rhythms can mediate neural coupling at distinct frequencies (26).

Our results demonstrate that PAC enables the lower frequency beta oscillations to modulate locally active interneurons and synchronously hold and release high-gamma activity in the different cycles of the slower oscillation. Such beta activities generated by high-level cortical areas therefore could harness the sensory-coding bottom-up signals, believed to be relayed using HG rhythms (6).

Top-down attention may recruit PAC for information transmission between cortical regions

Attention is controlled by a fronto-parietal network in human and nonhuman primates (33, 55). Recent studies have shown that top-down attention may enhance the cross-areal communication to route the most behaviorally relevant information between brain regions (11, 49, 50, 66). Other studies have revealed that PAC could facilitate this neuronal communication (7, 26, 53, 67). Importantly, electrophysiological studies have shown that top-down attention modulates PAC. For instance, the strength of coupling between the delta/theta (1–8 Hz) phase and gamma (30–120 Hz) power is reduced by attention in both the extra-striate and primary visual cortex (31, 32). We suggested that this suppression of delta-gamma PAC is linked to an enhancement of neural discrimination, suggestive of a role for PAC in modulating the neural representation of visual entities (32). Within the fronto-parietal network (rather the sensory areas), however another study showed that the coupling of theta phase (3–8 Hz) and beta (16–35 Hz)/gamma (>35 Hz) power is increased with the deployment of attention (29); where the authors suggest a role of PAC in inter-areal information transmission. In line with this, the strength of synchrony between theta (4–12 Hz) oscillations in the mice hippocampus and the gamma rhythms (30–70 Hz) in the medial prefrontal cortex is associated with behavioral performance in a working memory task (68). These studies are in line with our observation that PAC (between beta and HG) has a facilitatory role in high-level cognitive functions such as attention, presumably via contributing to the inter-areal communication (Fig. 7C). Together with our previous study (32), our results indicate that PAC may have different mechanistic roles at different frequencies; coupling between delta and gamma contributes to sensory representation, while coupling between beta and HG may improve information transmission.

Temporal dynamics of PAC might reflect the integration of sensory signals in time

Neurophysiological studies in humans and nonhuman primates have demonstrated that the neuronal activity in fronto-parietal areas subserves a cumulative process to guide behavior, temporally integrating sensory information arriving from upstream sensory areas (68). These studies have identified a signal-dependent neural buildup within frontal and parietal areas during the sensory-integration process (68–70). Specifically in parietal areas, different components of neural signals, including firing-rates (71), beta-band oscillations (22–30 Hz) (69), and centroparietal potentials (70) have been shown to undergo ramp-like changes corresponding to accumulation of the incoming sensory signals. The temporal pattern of these signals exhibit a gradual build-to-threshold dynamic, which predicts the behavioral response speed based on the slope of the temporal dynamic (69, 70). Some studies suggested that top-down influences such as attention can selectively gate inputs from upstream visual areas (e.g. MT and V4) (36) onto parietal cortex for underlying integrative representation of sensory information (70, 72). Based on previous studies documenting a long-range network reverberation in the beta band (10–26) (12, 15, 69, 73), our results indicate that the bottom-up beta-coupled high-gamma (180–220 Hz) activity is temporally regulated between different areas; a regulation that is under the influence of fronto-parietal areas, via processes like attention. Specifically, our observation that the strength of PAC long before the change event, determines the behavioral reaction time, may be indicative of a delay where PAC needs to establish a communication channel with downstream areas. In line with our previous observation that LFPs integrate longer in local networks (74), our results support the idea that LFP-based PAC might be an aid to allow a behaviorally efficient integration of information, by providing a sustained communication channel with downstream areas.

In light of recent challenges to the model of flexible routing through persistent cortical rhythms, as highlighted by Vinck et al. (75), our interpretations of beta and high-gamma oscillations' roles in the dorsal visual pathway merit reconsideration. Vinck et al. suggest that mechanisms like resonance and nonlinear integration could be crucial for cortical communication. While our data highlight the functional significance of PAC between beta and high-gamma oscillations in visuo-motor tasks, we must also consider the potential roles of aperiodic activities. Future research should investigate these dynamics comprehensively to enhance our understanding of neural communication and its implications for behavior. This integrated approach will refine our models and broaden the scope of our insights into cortical network functions.

Previously, we have suggested that a sensory area may consist of at least two distinct sub-networks; with a regulatory neural network gating the activity of the network of principal neurons. This gating is reflected by a coupling between the activities of the two networks (42). Our data confirm such gating influence of the local neuronal population activity in cortical areas processing visual information on the activity at the level of single neurons. We find that this gating is key to the flexible routing of sensory information through the visuo-motor networks and show that the influence of the oscillatory population activity (in the beta range) on single neurons is predictive of the behavioral performance. Similarly, the strength of the PAC between beta and high-gamma frequencies predicts behavioral performance. These findings demonstrate a unidirectional influence of network-level neural dynamics on the activity of single neurons to selectively pass on sensory information to downstream areas based on the behavioral need.

Materials and methods

Research with nonhuman primates represents a small but indispensable component of neuroscience research. The scientists in this study are aware and are committed to the great responsibility they have in ensuring the best possible science with the least possible harm to any animals used in scientific research (76, 77). The animals were group-housed with other macaque monkeys

in facilities of the German Primate Center in Goettingen, Germany in accordance with all applicable German and European regulations, as well as the Ethics Guidelines of the German Primate Center. The facility provides the animals with an enriched environment (incl. a multitude of toys and wooden structures (78, 79)), natural as well as artificial light, exceeding the size requirements of the European regulations, including access to outdoor conditions. We have established a comprehensive set of measures to ensure that the severity of our experimental procedures falls into the category of mild to moderate, according to the severity categorization of Annex VIII of the European Union's directive 2010/63/EU on the protection of animals used for scientific purposes (80). All animal procedures of this study have been approved by the responsible regional government office (Niedersaechsisches Landesamt fuer Verbraucherschutz und Lebensmittelsicherheit [LAVES]) under the permit numbers 33.42502/08-07.02 and 33.14.42502-04-064/07. For details of the animals' welfare and surgical procedures, see SI Appendix, Extended Methods. The details of the animal experiments, data analyses and computational modeling are provided in SI Appendix, Extended Methods.

Acknowledgments

We thank Laura Busse and Steffen Katzner for sharing the data they recorded from monkey T. We also thank Dirk Prüsse, Leonore Burchardt, and Ralf Brockhausen for superb technical assistance and the DPZ's veterinary and animal husbandry staff for their expert animal care.

Supplementary Material

Supplementary material is available at *PNAS Nexus* online.

Funding

S.T. acknowledges support from the Deutsche Forschungsgemeinschaft (DFG, German Research Foundation)—Projektnummer 154113120—SFB 889, project C04 and Research Unit 1847-A1 "Physiology of Distributed Computing Underlying Higher Brain Functions in Non-Human Primates" and Projektnummer 436260547 (NEURONEX). M.B.K. acknowledges support from the Iran Science Elites Federation Grant No 11/66332, and the Iranian Cognitive Sciences and Technologies Council (Grant 4225, to M.B.K.).

Author Contributions

Conceptualization: M.B.K., M.D., and M.E.; Methodology: M.B.K. and M.E.; Investigation: M.B.K.; Visualization: M.B.K.; Supervision: M.E., M.D., and S.T.; Writing original draft: M.B.K.; Review and editing: M.B.K., M.E., M.D., and S.T.

Data Availability

The data underlying the result figures are publicly available (81).

References

1 Parto Dezfouli M, Khamechian MB, Treue S, Esghaei M, Daliri MR. 2018. Neural activity predicts reaction in primates long before a behavioral response. *Front Behav Neurosci*. 12:207.
2 Khamechian MB, Kozyrev V, Treue S, Esghaei M, Daliri MR. 2019. Routing information flow by separate neural synchrony frequencies allows for "functionally labeled lines" in higher primate cortex. *Proc Natl Acad Sci U S A*. 2019;116(25):12506–12515.
3 Khamechian MB, Daliri MR. 2020. Decoding adaptive visuomotor behavior mediated by non-linear phase coupling in macaque area MT. *Front Neurosci*. 14:230.
4 Khamechian MB, Daliri MR. 2022. Frequency modulation of cortical rhythmicity governs behavioral variability, excitability and synchrony of neurons in the visual cortex. *Sci Rep*. 12:20914.
5 Schroeder CE, Lakatos P. 2009. Low-frequency neuronal oscillations as instruments of sensory selection. *Trends Neurosci*. 32: 9–18.
6 Siegel M, Donner TH, Oostenveld R, Fries P, Engel AK. 2007. High-frequency activity in human visual cortex is modulated by visual motion strength. *Cereb Cortex*. 17:732–741.
7 Lisman JE, Jensen O. 2013. The θ-γ neural code. *Neuron*. 77: 1002–1016.
8 Zareian B, *et al.* 2020. Attention strengthens across-trial pre-stimulus phase coherence in visual cortex, enhancing stimulus processing. *Sci Rep*. 10:4837.
9 Khodagholy D, Gelinas JN, Buzsáki G. 2017. Learning-enhanced coupling between ripple oscillations in association cortices and hippocampus. *Science*. 358:369–372.
10 Kucewicz MT, *et al.* 2014. High frequency oscillations are associated with cognitive processing in human recognition memory. *Brain*. 137:2231–2244.
11 Gregoriou GG, Gotts SJ, Zhou H, Desimone R. 2009. High-frequency, long-range coupling between prefrontal and visual cortex during attention. *Science* 324:1207–1210.
12 Kopell N, Ermentrout GB, Whittington MA, Traub RD. 2000. Gamma rhythms and beta rhythms have different synchronization properties. *Proc Natl Acad Sci U S A*. 97:1867–1872.
13 Hipp JF, Engel AK, Siegel M. 2011. Oscillatory synchronization in large-scale cortical networks predicts perception. *Neuron*. 69: 387–396.
14 Rohenkohl G, Bosman CA, Fries P. 2018. Gamma synchronization between V1 and V4 improves behavioral performance. *Neuron*. 100:953–963.e3.
15 Siegel M, Donner TH, Engel AK. 2012. Spectral fingerprints of large-scale neuronal interactions. *Nat Rev Neurosci*. 13:121–134.
16 Michalareas G, *et al.* 2016. Alpha-beta and gamma rhythms subserve feedback and feedforward influences among human visual cortical areas. *Neuron*. 89:384–397.
17 Bastos AM, *et al.* 2015. Visual areas exert feedforward and feedback influences through distinct frequency channels. *Neuron*. 85:390–401.
18 Richter CG, Thompson WH, Bosman CA, Fries P. 2017. Top-down beta enhances bottom-up gamma. *J Neurosci*. 37:6698–6711.
19 Smith JET, *et al.* 2015. Dynamics of the functional link between area MT LFPs and motion detection. *J Neurophysiol*. 114:80–98.
20 Meindertsma T, Kloosterman NA, Nolte G, Engel AK, Donner TH. 2017. Multiple transient signals in human visual cortex associated with an elementary decision. *J Neurosci*. 37:5744–5757.
21 Womelsdorf T, Fries P, Mitra PP, Desimone R. 2006. Gamma-band synchronization in visual cortex predicts speed of change detection. *Nature*. 439:733–736.
22 Liu J, Newsome WT. 2006. Local field potential in cortical area MT: stimulus tuning and behavioral correlations. *J Neurosci*. 26: 7779–7790.
23 Lee J, Lisberger SG. 2013. Gamma synchrony predicts neuron-neuron correlations and correlations with motor behavior in extrastriate visual area MT. *J Neurosci*. 33:19677–19688.
24 Davis ZW, Muller L, Reynolds JH. 2022. Spontaneous spiking is governed by broadband fluctuations. *J Neurosci*. 42:5159–5172.

25 Buzsáki G, Draguhn A. 2004. Neuronal oscillations in cortical networks. *Science*. 304:1926–1929.
26 Hyafil A, Giraud A-L, Fontolan L, Gutkin B. 2015. Neural cross-frequency coupling: connecting architectures, mechanisms, and functions. *Trends Neurosci*. 38:725–740.
27 Canolty RT, Knight RT. 2010. The functional role of cross-frequency coupling. *Trends Cogn Sci*. 14:506–515.
28 Jensen O, Colgin LL. 2007. Cross-frequency coupling between neuronal oscillations. *Trends Cogn Sci*. 11:267–269.
29 Fiebelkorn IC, Pinsk MA, Kastner S. 2018. A dynamic interplay within the frontoparietal network underlies rhythmic spatial attention. *Neuron*. 99:842–853.e8.
30 Wang L, Saalmann YB, Pinsk MA, Arcaro MJ, Kastner S. 2012. Electrophysiological low-frequency coherence and cross-frequency coupling contribute to BOLD connectivity. *Neuron*. 76:1010–1020.
31 Spyropoulos G, Bosman CA, Fries P. 2018. A theta rhythm in macaque visual cortex and its attentional modulation. *Proc Natl Acad Sci U S A*. 115:E5614–E5623.
32 Esghaei M, Daliri MR, Treue S. 2015. Attention decreases phase-amplitude coupling, enhancing stimulus discriminability in cortical area MT. *Front Neural Circuits*. 9:82.
33 Szczepanski SM, *et al.* 2014. Dynamic changes in phase-amplitude coupling facilitate spatial attention control in fronto-parietal cortex. *PLoS Biol*. 12:e1001936.
34 Doostmohammadi J, *et al.* 2023. Ripples in macaque V1 and V4 are modulated by top-down visual attention. *Proc Natl Acad Sci U S A*. 120:e2210698120.
35 Aboutorabi E, *et al.* 2024. Phase of neural oscillations as a reference frame for attention-based routing in visual cortex. *Prog Neurobiol*. 233:102563.
36 Ray SB, Kaping D, Treue S. 2021. Feature-based gating of cortical information transmission. bioRxiv 2021.10.08.463709. https://doi.org/10.1101/2021.10.08.463709, preprint: not peer reviewed.
37 Mehrpour V, Martinez-Trujillo JC, Treue S. 2020. Attention amplifies neural representations of changes in sensory input at the expense of perceptual accuracy. *Nat Commun*. 11:2128.
38 Kozyrev V, Daliri MR, Schwedhelm P, Treue S. 2019. Strategic deployment of feature-based attentional gain in primate visual cortex. *PLoS Biol*. 17:e3000387.
39 Esghaei M, Daliri MR. 2014. Decoding of visual attention from LFP signals of macaque MT. *PLoS One*. 9:e100381.
40 Katzner S, Busse L, Treue S. 2009. Attention to the color of a moving stimulus modulates motion-signal processing in macaque area MT: evidence for a unified attentional system. *Front Syst Neurosci*. 3:12.
41 Voytek B, D'Esposito M, Crone N, Knight RT. 2013. A method for event-related phase/amplitude coupling. *Neuroimage*. 64: 416–424.
42 Esghaei M, Treue S, Vidyasagar TR. 2022. Dynamic coupling of oscillatory neural activity and its roles in visual attention. *Trends Neurosci*. 45:323–335.
43 Siapas AG, Lubenov EV, Wilson MA. 2005. Prefrontal phase locking to hippocampal theta oscillations. *Neuron*. 46:141–151.
44 Esghaei M, Daliri MR, Treue S. 2018. Attention decouples action potentials from the phase of local field potentials in macaque visual cortical area MT. *BMC Biol*. 16:86.
45 Cohen MR, Maunsell JHR. 2009. Attention improves performance primarily by reducing interneuronal correlations. *Nat Neurosci*. 12:1594–1600.
46 Daliri MR, Kozyrev V, Treue S. 2016. Attention enhances stimulus representations in macaque visual cortex without affecting their signal-to-noise level. *Sci Rep*. 6:27666.
47 Busse L, Katzner S, Tillmann C, Treue S. 2008. Effects of attention on perceptual direction tuning curves in the human visual system. *J Vis*. 8:2.1–213.
48 Xue C, Kaping D, Ray SB, Krishna BS, Treue S. 2017. Spatial attention reduces burstiness in macaque visual cortical area MST. *Cereb Cortex*. 27:83–91.
49 Briggs F, Mangun GR, Usrey WM. 2013. Attention enhances synaptic efficacy and the signal-to-noise ratio in neural circuits. *Nature*. 499:476–480.
50 Morishima Y, *et al.* 2009. Task-specific signal transmission from prefrontal cortex in visual selective attention. *Nat Neurosci*. 12: 85–91.
51 Carrasco M. 2011. Visual attention: the past 25 years. *Vision Res*. 51:1484–1525.
52 Gregoriou GG, Paneri S, Sapountzis P. 2015. Oscillatory synchrony as a mechanism of attentional processing. *Brain Res*. 1626:165–182.
53 von Nicolai C, *et al.* 2014. Corticostriatal coordination through coherent phase-amplitude coupling. *J Neurosci*. 34:5938–5948.
54 Grabenhorst M, Michalareas G, Maloney LT, Poeppel D. 2019. The anticipation of events in time. *Nat Commun*. 10:5802.
55 Buschman TJ, Miller EK. 2007. Top-down versus bottom-up control of attention in the prefrontal and posterior parietal cortices. *Science*. 315:1860–1862.
56 Dann B, Michaels JA, Schaffelhofer S, Scherberger H. 2016. Uniting functional network topology and oscillations in the fronto-parietal single unit network of behaving primates. *Elife*. 5:e15719.
57 Donner TH, *et al.* 2007. Population activity in the human dorsal pathway predicts the accuracy of visual motion detection. *J Neurophysiol*. 98:345–359.
58 Bastos AM, *et al.* 2012. Canonical microcircuits for predictive coding. *Neuron*. 76:695–711.
59 van Pelt S, *et al.* 2016. Beta- and gamma-band activity reflect predictive coding in the processing of causal events. *Soc Cogn Affect Neurosci*. 11:973–980.
60 Bragin A, Engel J, Wilson CL, Fried I, Buzsáki G. 1999. High-frequency oscillations in human brain. *Hippocampus*. 9:137–142.
61 Stark E, *et al.* 2014. Pyramidal cell-interneuron interactions underlie hippocampal ripple oscillations. *Neuron*. 83:467–480.
62 Suffczynski P, Crone NE, Franaszczuk PJ. 2014. Afferent inputs to cortical fast-spiking interneurons organize pyramidal cell network oscillations at high-gamma frequencies (60–200 Hz). *J Neurophysiol*. 112:3001–3011.
63 Billeke P, *et al.* 2017. Brain state-dependent recruitment of high-frequency oscillations in the human hippocampus. *Cortex*. 94:87–99.
64 Dragoi G, Tonegawa S. 2011. Preplay of future place cell sequences by hippocampal cellular assemblies. *Nature*. 469:397–401.
65 Singer AC, Carr MF, Karlsson MP, Frank LM. 2013. Hippocampal SWR activity predicts correct decisions during the initial learning of an alternation task. *Neuron*. 77:1163–1173.
66 Esghaei M, Martínez-Trujillo J, Treue S. 2024. Dissecting attention: rate modulation vs. phase modulation. *Neuron*. 112:2263–2264.
67 Tamura M, Spellman TJ, Rosen AM, Gogos JA, Gordon JA. 2017. Hippocampal-prefrontal theta-gamma coupling during performance of a spatial working memory task. *Nat Commun*. 8:2182.
68 Hanks TD, Summerfield C. 2017. Perceptual decision making in rodents, monkeys, and humans. *Neuron*. 93:15–31.
69 O'Connell RG, Dockree PM, Kelly SP. 2012. A supramodal accumulation-to-bound signal that determines perceptual decisions in humans. *Nat Neurosci*. 15:1729–1735.

70 Kelly SP, O'Connell RG. 2013. Internal and external influences on the rate of sensory evidence accumulation in the human brain. *J Neurosci*. 33:19434–19441.
71 Roitman JD, Shadlen MN. 2002. Response of neurons in the lateral intraparietal area during a combined visual discrimination reaction time task. *J Neurosci*. 22:9475–9489.
72 Ibos G, Freedman DJ. 2014. Dynamic integration of task-relevant visual features in posterior parietal cortex. *Neuron*. 83:1468–1480.
73 Wang X-J. 2002. Probabilistic decision making by slow reverberation in cortical circuits. *Neuron*. 36:955–968.
74 Esghaei M, Daliri MR, Treue S. 2017. Local field potentials are induced by visually evoked spiking activity in macaque cortical area MT. *Sci Rep*. 7:17110.
75 Vinck M, *et al*. 2023. Principles of large-scale neural interactions. *Neuron*. 111:987–1002.
76 Roelfsema PR, Treue S. 2014. Basic neuroscience research with nonhuman primates: a small but indispensable component of biomedical research. *Neuron*. 82:1200–1204.
77 Treue S, Lemon R. 2023. The indispensable contribution of nonhuman primates to biomedical research. In: Robinson LM, Weiss A, editors. *Nonhuman primate welfare: from history, science, and ethics to practice*. Cham: Springer. p. 589–603.
78 Berger M, *et al*. 2018. Standardized automated training of rhesus monkeys for neuroscience research in their housing environment. *J Neurophysiol*. 119:796–807.
79 Calapai A, *et al*. 2017. A cage-based training, cognitive testing and enrichment system optimized for rhesus macaques in neuroscience research. *Behav Res Methods*. 49:35–45.
80 Pfefferle D, Plümer S, Burchardt L, Treue S, Gail A. 2018. Assessment of stress responses in rhesus macaques (*Macaca mulatta*) to daily routine procedures in system neuroscience based on salivary cortisol concentrations. *PLoS One*. 13:e0190190.
81 Khamechian MB, Daliri MR, Treue S, Esghaei M. 2024 Data from "Coupled oscillations orchestrate selective information transmission in visual cortex (Data underlying result figures)". https://doi.org/10.6084/m9.figshare.26250083.v1 (July 11, 2024).